Methods and Applications in Fluorescence

**PAPER** • **OPEN ACCESS**

# Dual color single particle tracking via nanobodies

To cite this article: David Albrecht *et al* 2015 *Methods Appl. Fluoresc.* **3** 024001

Methods and Applications in Fluorescence

PAPER

# Dual color single particle tracking via nanobodies

David Albrecht[1,3,4], Christian M Winterflood[1,4] and Helge Ewers[1,2]

[1] Randall Division of Cell and Molecular Biophysics, King's College London, SE1 1UL, UK
[2] Institut für Chemie und Biochemie, Freie Universität Berlin, Thielallee 63, 14195 Berlin, Germany
[3] Institute of Biochemistry, Department of Biology, ETH Zurich, Switzerland

**E-mail:** helge.ewers@kcl.ac.uk

**Keywords:** single particle tracking, nanobody, single molecule, mHoneydew

OPEN ACCESS

RECEIVED
14 October 2014

REVISED
7 January 2015

ACCEPTED FOR PUBLICATION
12 January 2015

PUBLISHED
27 March 2015



## Abstract

Single particle tracking is a powerful tool to investigate the function of biological molecules by following their motion in space. However, the simultaneous tracking of two different species of molecules is still difficult to realize without compromising the length or density of trajectories, the localization accuracy or the simplicity of the assay. Here, we demonstrate a simple dual color single particle tracking assay using small, bright, high-affinity labeling via nanobodies of accessible targets with widely available instrumentation. We furthermore apply a ratiometric step-size analysis method to visualize differences in apparent membrane viscosity.

S Online supplementary data available from stacks.iop.org/MAF/3/024001

## 1. Introduction

Single particle tracking (SPT) is a powerful tool for the investigation of the lateral motion of biological molecules in lipid bilayers such as membranes. Based on the connection of spatial positions of single particles or molecules detected at nanometer accuracy over time, SPT allows the quantitative description of the motion of single molecules or larger particles. Besides giving access to the diffusion coefficient, the focus on a single particle allows the analysis of specific events that are not detectable in ensemble measurements, often at nanoscopic resolution and in correlation to other structures present in the sample. As a result, globally important phenomena can be deduced from the repeated investigation and detailed statistic analysis of single events. Following this principle, SPT has been instrumental in exploring the structural difference between the cellular plasma membrane and ideal lipid bilayers [1–3], and in generally demonstrating the interaction of membrane molecules with cytoskeletal scaffolds [4, 5] (for excellent reviews, see [6–9]). Problems still intractable due to technical limitations may be expected to become accessible based on new detection methods [10–12], the development of novel labeling reagents [13–15] and analysis methods [16–18]. Recently, assays such as uPAINT [19] or sptPALM [20] have allowed the generation of hundreds of trajectories in a short amount of time and thereby opened the door to efficient and detailed mapping of interaction sites of membrane molecules with submembrane scaffolds and their functional characterization [5, 21–23]. The next necessary step is the combination of such new developments with dual color imaging, so that dependencies or interactions between molecules can be investigated. Recently, a number of dual color assays have been developed using quantum dots coupled to the cell surface via antibodies [24–26] or two spectrally separated fluorescent photoactivatable proteins in sptPALM [27]. However, these assays are limited by the requirement of complex instrumentation (in dual color sptPALM, three laser lines have to be used simultaneously in TIRF mode) and labels with undesirable properties such as the relatively large quantum dots or the comparably low photon yield of fluorescent proteins.

Here, we demonstrate a method for dual color high-density SPT via nanobodies. Our method relies on the expression of recombinant constructs labeled with fluorescent proteins, which are used as epitopes for the binding of small high-affinity binders, so-called nanobodies, as probes. By making use of the fluorescent proteins GFP or YFP and mHoneydew [28] which are of different evolutionary descent but possess similar spectral properties, we free the orange-red and far red parts of the spectrum to be used for bright organic dyes coupled to the nanobodies, making our assay easily accessible in

[4] David Albrecht and Christian M Winterflood contributed equally to this work.

relatively simple setups. We furthermore suggest ratiometric mapping of the relative step-size of two different probes to characterize cellular plasma membranes.

## 2. Experimental details

### 2.1. Molecular cloning of probes

The transmembrane probe L-YFP-GT46, a custom designed construct used as a membrane marker containing an extracellular YFP and a short cytoplasmic tail was a kind gift of Patrick Keller [29] and the GFP-GPI construct was a kind gift from the Helenius laboratory [29]. To simplify molecular cloning procedures the amino acid sequence of mHoneydew [28] was modified to include the N-terminus of EGFP, MVSKGEE, followed by a spacer NNMA, and the C-terminus, GMDELYK, respectively, (figure 1(*a*)). Adjustment of the termini was previously reported to improve the fluorescence properties of fusion constructs and is found in other DsRed derived fluorophores as well [28]. The amino acid sequence was reverse translated into cDNA applying *Rattus norvegicus* codon usage and synthesized (Centic Biotec). The constructs containing mHoneydew were generated by exchanging the GFP or YFP moiety for mHoneydew by restriction digestion and ligation via the unique AgeI and BsrGI sites that flank the respective fluorophores.

### 2.2. Nanobody labeling

Anti-GFP- and anti-RFP nanobodies (Chromotek) were labeled with Cy3B (Life Sciences) and Atto647N (Atto-Tec) by standard N-hydroxysuccinimidyl ester chemistry according to the manufacturer's protocol using a 5-fold molar excess of dye giving a dye to nanobody ratio of ~1.5. The labeled nanobody was purified from the excess of unreacted dye using three 3 kDa MWCO desalting columns (Zeba Spin, Thermo Fisher). The labeling ratio was determined by absorption spectrometry according to the manufacturer's labeling protocol. The anti-RFP nanobodies were labeled and stored in the presence of 15% (v/v) DMSO to prevent precipitation.

### 2.3. Cell culture and transfection

Human osteosarcoma U2OS cells and normal rat kidney epithelial cells (NRK-52E) were grown in low glucose DMEM without phenol red supplemented with 10% fetal bovine serum, penicillin, streptomycin and GlutaMAX (all Life Technologies) at 37 °C in a $CO_2$-controlled humidified incubator. Cells were transferred to round 18 mm diameter #1.0 glass coverslips (Fisher Scientific) and transiently transfected using Lipofectamine 2000 (Life Technologies). Images were acquired 18–48 h after transfection.

### 2.4. Fluorescence microscopy

Immunofluorescence microscopy was performed on a spinning-disk confocal setup (Roper Scientific) on an inverted Olympus IX71. Single particle tracking was performed on a custom-built setup. In brief, a 473 nm laser (100 mW, Laserglow Technologies), a 556 nm (200 mW, Laserglow Technologies) and a 643 nm laser (150 mW, Toptica Photonics) were focused onto the back-focal plane of an Olympus NA 1.49, 60x, TIRF-objective. A quad-edge dichroic beamsplitter (405/488/532/635 nm, Semrock) was used to separate fluorescence emission from excitation light.

Emission light was filtered by a quad-band bandpass filter (446/523/600/677 nm, Semrock). A longpass dichroic beamsplitter (635 nm, Semrock) was used to separate Cy3B fluorescence from Atto647N fluorescence and the separated emission beams were additionally filtered by bandpass filters (Cy3B emission: 607/70 nm, Semrock, Atto647N: 700/75 nm, Chroma). The emission light was focused by two separate 500 mm tube lenses onto a back-illuminated EM-CCD chip (Evolve, Photometrics) which was water-cooled to −80 °C.

#### 2.4.1. *Single particle tracking experiments*

Single particle tracking in live cells was performed in live-cell imaging buffer (145 mM NaCl, 5 mM KCl, 10 mM Glucose,10 mM HEPES, 2 mM $CaCl_2$, 1 mM $MgCl_2$, 0.2% (w/v) BSA, 10 mM ascorbate, [30]). The microscope stage was kept at 37 °C. Nanobodies were added immediately prior to image acquisition at a concentration of ~25 pM and multiple image series (typically 10–20) of 500 frames were recorded with 25 ms exposure time and 5 ms laser illumination time.

#### 2.4.2. *Data analysis*

All data analysis was performed in MATLAB (Mathworks). Single particle positions were determined by Gaussian fitting based on a maximum likelihood estimator [31]. The lateral localization accuracy was ~10–15 nm. For each track a diffusion coefficient $D$ was calculated from the mean square displacement (MSD) using the following relationship:

$$\mathrm{MSD}(t) = \langle r^2 \rangle = 4 \cdot D \cdot t$$

where $r^2$ is $(x_{i+1} - x_i)^2 + (y_{i+1} - y_i)^2$ in the $i$th frame, $D$ is the diffusion coefficient and $t$ is the elapsed time between two successive frames. The diffusion coefficient $D$ was calculated from the slope of a linear fit through the points $i = 2$ to $i = 4$ of the MSD plotted versus $t$. Only trajectories with a minimum length of 5 consecutive frames were considered for analysis. Nanobodies bound to the coverglass exhibited a $D$ of $\leq 10^{-4}\,\mu\mathrm{m}^2\,\mathrm{s}^{-1}$ and were excluded from further analysis.

#### 2.4.3. *Diffusion mapping*

Diffusion maps of cells were generated by calculating the step-size between two consecutive localizations within the same track. The average position of the two consecutive localizations was assigned the value of the step-size. The $xy$-positions were converted to pixels and all step-sizes within the same pixel were averaged to obtain the value of the step-size for the corresponding pixel.

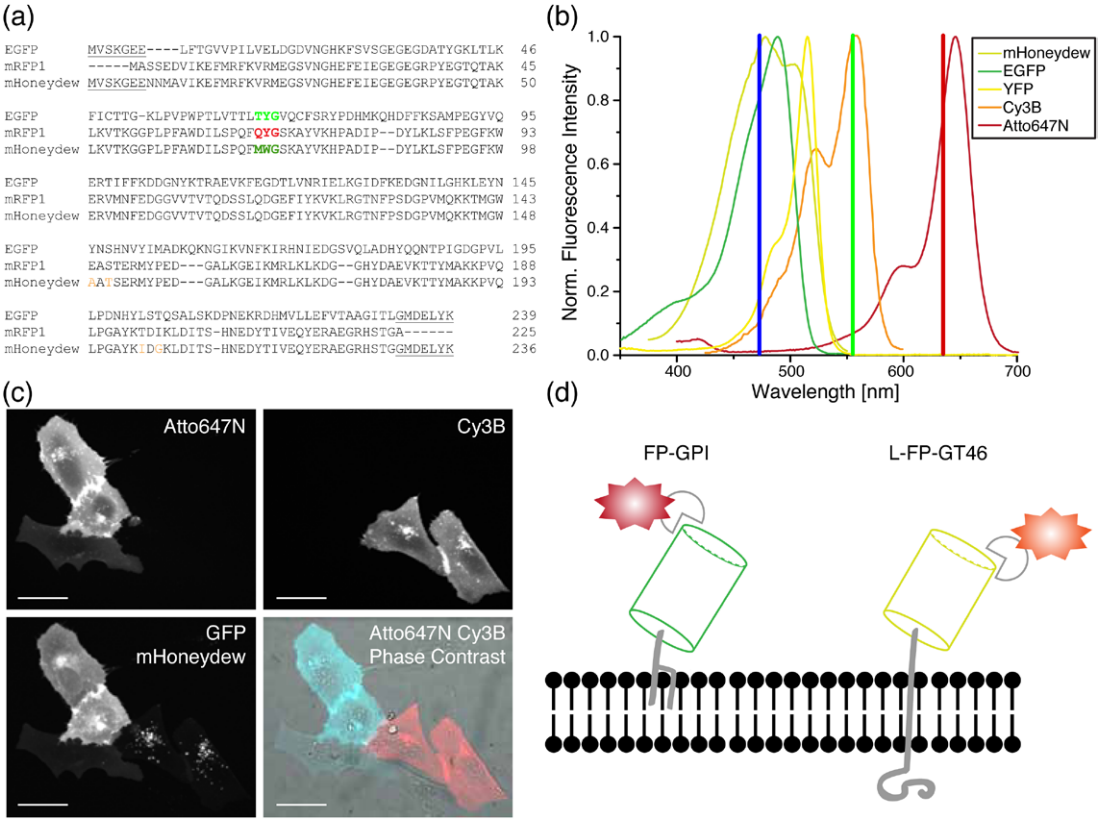


**Figure 1.** Dual color labeling of GFP and mHoneydew using anti-GFP and anti-RFP nanobodies. (*a*) Amino acid sequence alignment of EGFP, mRFP1 and mHoneydew, the fluorophores are emphasized in corresponding colors. The underlined sequences were incorporated into the mHoneydew sequence to facilitate cloning procedures. (*b*) Normalized excitation spectra of the fluorescent proteins and organic dyes used in this study. Blue, green and red lines represent commonly used laser lines in the blue, yellow–green and red spectral range. (*c*) Fluorescence micrographs of cultures containing cells that express either GFP-GPI detected via Atto647N-labeled anti-GFP nanobodies or L-mHoneydew-GT46 detected by Cy3B-labeled anti-RFP nanobodies. Shown are the far red, orange–red and green fluorescence detection channels and a merged image of the far red and orange–red detection channels with a phase contrast image. (*d*) Illustration representing the two membrane probes. Left: FP-GPI coupled to Atto647N-anti-GFP. This molecule resides in the outer leaflet of the plasma membrane. Right: L-FP-GT46 coupled to Cy3B-anti-RFP nanobody. L-mHoneydew-GT46 is a transmembrane protein with a short cytoplasmic tail. Scale bars are 10 $\mu$m.

#### 2.4.4. *Image registration*

To overlay the orange–red and far red channels used for SPT, multi-color fiduciary markers were employed (100 nm diameter Tetraspeck beads, Life Technologies). A calibration image of the beads was recorded to calculate a transformation matrix. The transformation matrix was calculated with the MATLAB (Mathworks) built-in routine cp2tform using an affine transformation. This corrects for field distortions, differences in chromatic aberration, as well as differences in magnification due to differences in the optical path length for the light transmitted or reflected by the dichroic beamsplitter. The method was tested by calculating a transformation matrix from a set of randomly distributed beads adsorbed to a coverslip and applying this transformation matrix to another set of beads on a different coverslip (data not shown). From this we determined a registration error of less than 30 nm across the entire field of view.

## 3. Results and discussion

### 3.1. Dual color labeling via nanobodies

The commercially available anti-GFP and anti-RFP nanobodies bind variants of jellyfish *Aquorea victoria* GFP [32] such as EGFP and YFP and variants of the coral *Discosoma sp.* DsRed [33] such as mRFP and mCherry, respectively. They thus allow targeting two spectrally well-separated fluorophores in the green and orange–red parts of the spectrum. To use these nanobodies with two bright organic dyes useful for single molecule tracking, we aimed to free the orange–red part of the spectrum to allow dual color tracking with orange–red and far red dye pairs such as Cy3/Cy5 or Atto565/647N. To do so, we made use of mHoneydew, a further permutation of mRFP that exhibits low brightness and like EGFP covers the green part of the spectrum (figure 1(*a*), [28]). Neither EGFP, YFP nor mHoneydew are excitable by the 556 nm laser line, which frees the orange–red and far red channels while avoiding background fluorescence from off-target excitation of the fluorescent proteins (figure 1(*b*)).

We added anti-GFP and anti-RFP nanobodies labeled with Atto647N and Cy3B, respectively, to live cells transfected with both L-mHoneydew-GT46 and GFP-GPI, two membrane-anchored probes that are tagged on their extracellular domains. Anti-GFP nanobodies bound specifically to cells expressing GFP-GPI,

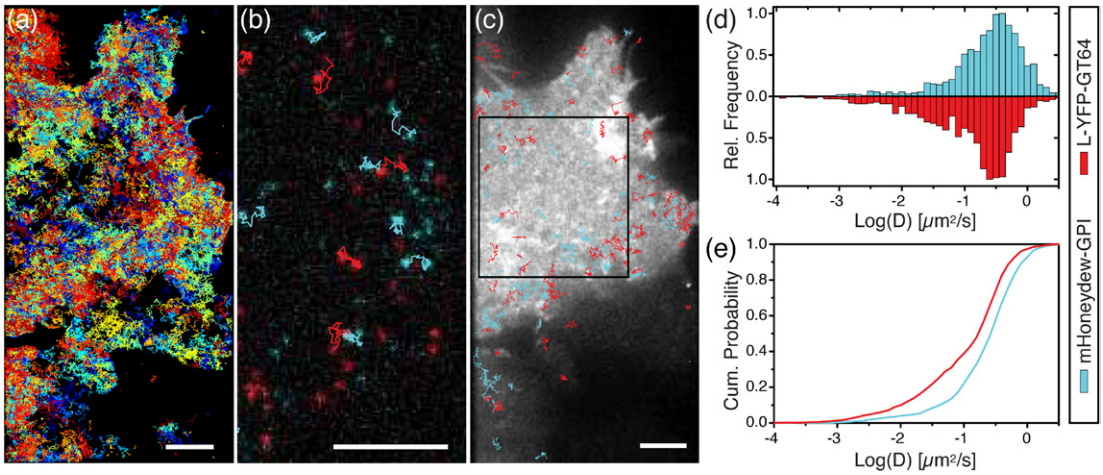


**Figure 2.** Dual color single-particle tracking of mHoneydew-GPI and L-YFP-GT46 in U2OS cells. (*a*) Fluorescence micrograph of live cells expressing L-YFP-GT46 overlaid with trajectories longer than 5 frames (4920 trajectories) gathered in an anti-GFP nanobody uPAINT experiment. (*b*) Live-cell dual color SPT experiment. Shown is a dual color fluorescence micrograph merged between two timepoints ~0.75 s apart. The trajectories generated from connected particle positions over the 25 frame acquisition period between these timepoints are overlaid in blue (mHoneydew-GPI) and red (L-YFP-GT46), respectively. (*c*) Fluorescence micrograph of the YFP fluorescence of a cell overlaid with an equal number of mHoneydew-GPI and L-YFP-GT46 trajectories of track lengths of 30–40 frames. (*d*) Histograms and (*e*) cumulative probability plots of diffusion coefficients for tracks with a minimum track-length of 5 steps from the area outlined by the box in (*b*) for a total of 1108 tracks for mHoneydew-GPI (blue) and 1345 tracks for L-YFP-GT46 (red). L-YFP-GT46 molecules exhibited a mean and median diffusion coefficient $D$ of 0.27 and 0.17 $\mu m^2 s^{-1}$, respectively. Nanobodies coupled to mHoneydew-GPI exhibited a mean and median $D$ of 0.42 and 0.26 $\mu m^2 s^{-1}$, respectively. Scale bars are 5 $\mu$m.

but not to untransfected cells, while the anti-RFP nanobodies exclusively labeled cells expressing L-mHoneydew-GT46 (figure 1(*c*)). We noted that while mHoneydew-fluorescence in the green fluorescence channel was significantly weaker than that of GFP, transfected cells could still be identified based on fluorescence (figure 1(*c*), 2nd panel).

We thus established a system in which two differentially detectable fluorescent proteins are anchored in the membrane by structurally distinct membrane anchors. While the lipidic glycosylphosphatidylinositol (GPI)-anchor tethers a fluorescent protein fusion construct (FP-GPI) to the outer leaflet of the plasma membrane, the L-FP-GT46 construct is connected to the plasma membrane via the single-spanning transmembrane domain of the LDL-receptor (figure 1(*d*)). Both molecules have been developed as standards to represent typical membrane molecules and have been widely applied in biophysical studies of membrane protein motion. It has consistently been found that GPI-anchored molecules exhibit a diffusion coefficient that is significantly higher than that of single-spanning transmembrane molecules [34, 35]. We thus expected these molecules to react differently to viscous properties of the plasma membrane brought about by protein density, the submembrane cytoskeleton or dynamic changes in local lipid composition.

### 3.2. Dual color single particle tracking

We next performed simultaneous dual color SPT of mHoneydew-GPI and L-YFP-GT46 molecules in the plasma membrane of live cells using the uPAINT method [19]. In uPAINT, a low concentration of fluorescent ligands is introduced into the medium prior to the image acquisition. From this constant pool fluorescent ligands continuously bind to the membrane-integrated probes at a constant rate and are tracked until photobleached, thus yielding a large number of tracking events. Background fluorescence from unbound ligands is largely avoided due to their rapid movement and due to imaging in total internal reflection fluorescence (TIRF) mode. When we added Cy3B-labeled anti-RFP and Atto647N-labeled anti-GFP nanobodies at picomolar concentrations to transfected U2OS cells, we observed binding of individual nanobodies as discrete, mobile spots at the basal membrane of transfected cells within seconds (see Supplementary Movie 1) (stacks.iop.org/MAF/3/024001). A large number of fluorescent nanobodies could be localized on the membrane in both fluorescence channels, most of which were found to be mobile on the observed timescale (figures 2(*a*) and (*b*)). When we tracked the resulting localizations of single molecules in the plane of the membrane over time, we yielded track lengths of 15–20 steps on average both for Cy3B-labeled anti-RFP nanobodies and for Atto647N-labeled anti-GFP nanobodies. As expected, mHoneydew-GPI molecules exhibited a larger diffusion coefficient than L-YFP-GT46 (figures 2(*c*)–(*e*)). Specifically, the mean/median diffusion coefficients ($D$) of mHoneydew-GPI and L-YFP-GT46 were 0.42/0.26 $\mu m^2 s^{-1}$ (1108 tracks) and 0.27/0.17 $\mu m^2 s^{-1}$ (1345 tracks), respectively. With our proposed method it was therefore possible to detect the difference in mobility exhibited between a lipid-anchored and a transmembrane-anchored molecule in the cellular plasma membranes.

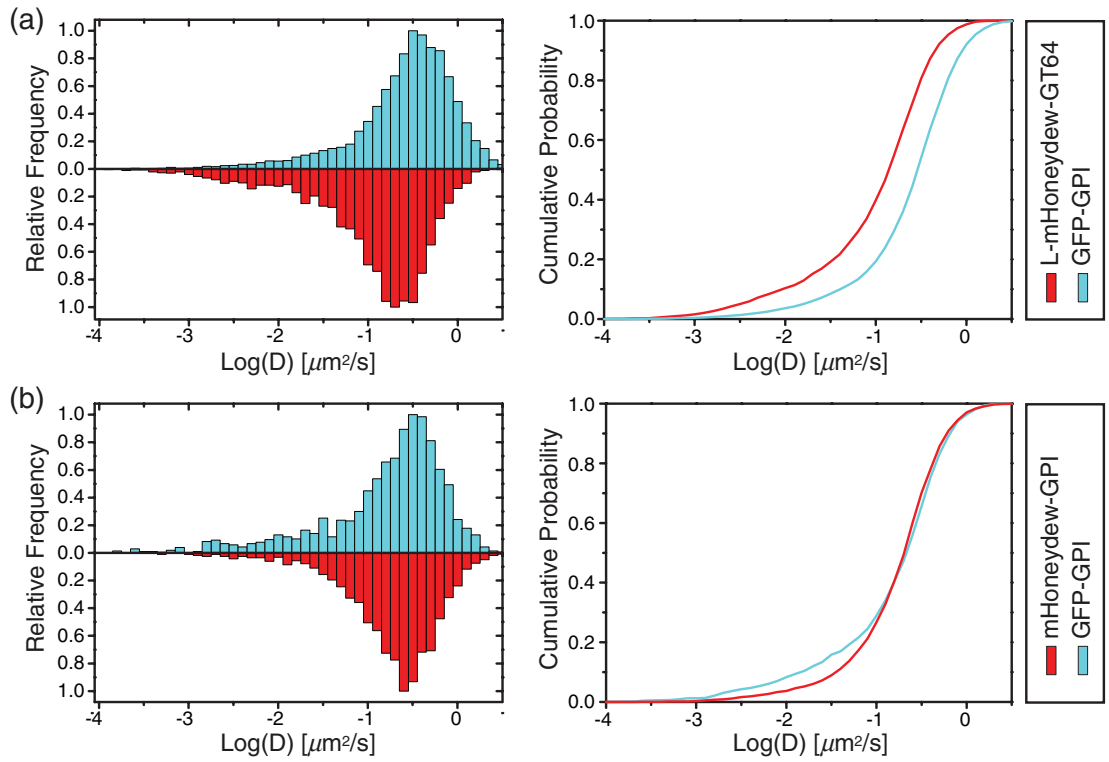


**Figure 3.** Controls of membrane diffusivity measurements. (*a*) Mobility of GFP-GPI (blue) and L-mHoneydew-GT46 (red) in the plasma membrane of an NRK52E cell. Shown are a histogram (left) and a cumulative probability plot (right) for a single cell of the diffusion coefficient $D$ with a mean/median of 0.46/0.29 $\mu m^2 s^{-1}$ (12 670 tracks) for GFP-GPI and 0.22/0.14 $\mu m^2 s^{-1}$ for L-mHoneydew-GT46 (4158 tracks). (*b*) Mobility of GFP-GPI (blue) and mHoneydew-GPI (red) in the plasma membrane of a NRK52E cell. Shown are a histogram (left) and a cumulative probability plot (right) for a single cell of $D$ with a mean/median of 0.33/0.22 $\mu m^2 s^{-1}$ for GFP-GPI (2583 tracks) and 0.32/0.21 $\mu m^2 s^{-1}$ for mHoneydew-GPI (2119 tracks).

To generalize our conclusions, we used the NRK52E cell line and tested whether the observed difference in diffusivity was found in different cell lines as well. NRK52E cells were transfected with GFP-GPI and L-mHoneydew-GT46. In these cells the GPI-anchored probe displayed a higher mobility compared to the transmembrane probe as well. However, this difference was more pronounced with a mean/median $D$ of 0.46/0.29 $\mu m^2 s^{-1}$ (12 670 tracks) and 0.22/0.14 $\mu m^2 s^{-1}$ (4158 tracks) (figure 3(*b*)) for the GPI-anchored and the transmembrane probe, respectively. In U2OS cells the transmembrane probe consistently showed a higher mobility compared to NRK52E cells.

To test whether the nature of the binding epitope influenced membrane mobility, we cotransfected GFP-GPI and mHoneydew-GPI in NRK52E cells and performed dual color SPT using the same anti-GFP-Atto647N and anti-RFP-Cy3B nanobodies. In this case both probes exhibited an almost identical distribution of diffusion coefficients (figure 3(*b*)). The mean/median diffusion coefficients ($D$) of GFP-GPI and mHoneydew-GPI were very similar with 0.33/0.22 $\mu m^2 s^{-1}$ (2583 tracks) and 0.32/0.21 $\mu m^2 s^{-1}$ (2119 tracks), respectively. However, we observed a small fraction of tracks with low mobility for GFP-GPI that we did not observe with mHoneydew-GPI. This fraction may represent low mobility anti-GFP Atto647N-nanobodies attached to GFP in cell debris. This was only a small fraction of particles and the labeling epitope did not seem to have an effect on membrane mobility as the distribution of mobile particles was nearly identical.

### 3.3. Diffusion mapping of membrane molecules

While the cumulative distribution of diffusion coefficients of all trajectories allows the comparison and analysis of the overall population of particles, at the same time, due to the high density of trajectories our method allows to see if diffusivity of membrane molecules is consistently the same in all areas of the cell [20] or if local inhomogeneities in membrane viscosity are experienced differently by the two membrane probes. To this end, the GPI-anchored probe may serve as a reference probe, which accounts for membrane composition as well as protein crowding effects [36], while the GT46 transmembrane protein may additionally experience physical obstacles by the submembrane cytoskeleton via its intracellular moiety [37]. Figure 4(*a*) shows mobility maps in terms of the average step-size between two subsequent frames as exhibited by mHoneydew-GPI and L-YFP-GT46. In some areas, an insufficient number of molecules to generate a statistically reliable average step-size were measured. Such pixels were left void. This was especially the case for the center of the cell as the nanobodies mainly bound at the edges and apical part of the cell and

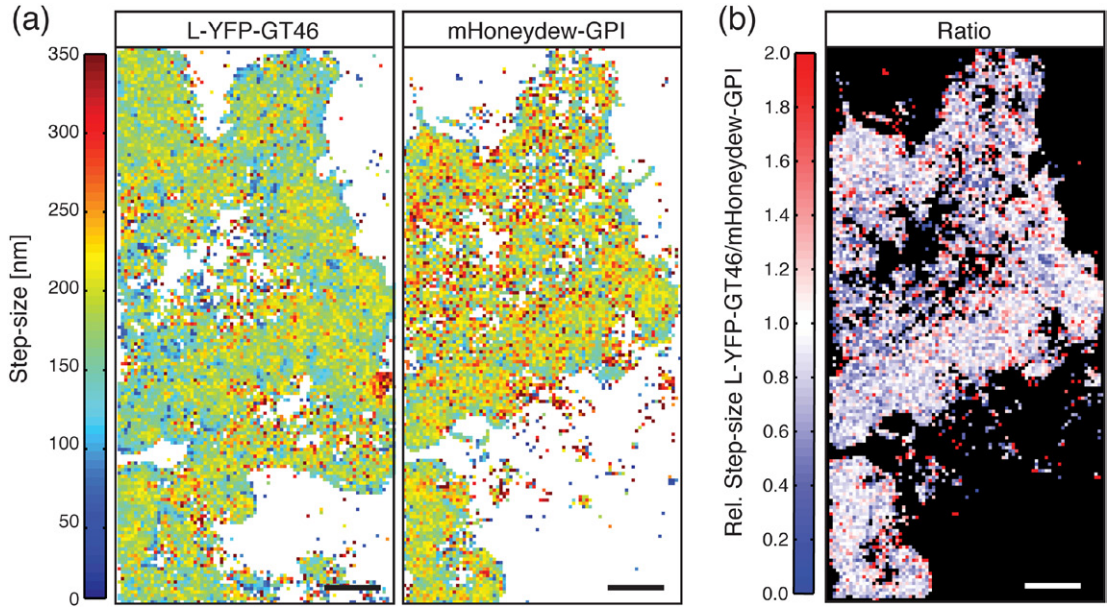


**Figure 4.** Mapping of protein mobility of cell membranes. (*a*) Heatmaps of the average 25 ms step-size for an acquisition of >5000 frames. Shown are heatmaps for the cell in figure 2(*b*) for the transmembrane molecule L-YFP-GT46 (left) and the lipid-anchored mHoneydew-GPI (right). (*b*) Map of relative step-sizes. Shown is the ratio between the average step-size of L-YFP-GT46 with respect to mHoneydew-GPI created from the maps in (*a*). Pixels are 288 nm (3 × 3 camera pixels), scale bars are 5 $\mu$m.

thus most fluorophores photobleached before reaching the center of the cell. The mobility maps show that for both mHoneydew-GPI and L-YFP-GT46 diffusion was relatively slower at the cell edges and relatively faster in areas several µm away from the cell edge (figure 4(*a*)) as previously reported [19].

The precise registration of the two fluorescence channels afforded the generation of a ratiometric map as shown in figure 4(*b*). Here, we plotted the ratio of step-sizes of L-YFP-GT46/mHoneydew-GPI to visualize regions with different relative mobility between the GPI-anchored and the transmembrane probe. In the ratiometric map, areas where the step-sizes of the GPI-anchored molecule are relatively shorter than for the transmembrane molecule are represented in red, while where the step-size of the GPI-anchored molecule is relatively longer, the pixel is represented in blue. For the majority of the plasma membrane area the ratio is slightly below 1 (white to light blue areas in figure 4(*b*)), meaning that the molecules exhibit very similar step-sizes. However, there were regions of up to 1–2 $\mu$m in diameter in which the step-sizes for the GPI-anchored molecules seemed significantly higher (blue areas in figure 4(*b*)). The transmembrane molecules exhibited a longer average step-size only in small isolated areas (red areas in figure 4(*b*)). These findings show that given further statistical analysis and a high amount of data our assay in the future may be capable of detecting areas in which the membrane influences the mobility of transmembrane and lipid-anchored molecules differently.

## 4. Conclusion

We demonstrate here a dual color SPT assay that can be executed with commonly used excitation lasers and the corresponding filter sets. Based on this assay, we describe a simple method to measure local differences in the viscosity of the plasma membrane based on the simultaneous tracking of membrane proteins that are incorporated into the plasma membrane by different membrane anchors.

Our method allows for the fast acquisition of hundreds of single molecule trajectories resulting in a high area coverage and combines excellent specificity with the possibility to track two proteins of interest simultaneously. Since we generate hundreds of trajectories with thousands of steps, we achieve high-density coverage of steps on the cellular membrane within few minutes, making this approach feasible for use with membrane perturbations. By mapping the average step-size for a given molecule for each pixel on the entire cell, we can identify areas of decreased or increased apparent membrane viscosity experienced by that molecule. By employing ratiometric mapping of the relative difference between the step-size of the GPI-anchored and the transmembrane molecule, we may be able to ask in future experiments, what the nature of such areas is and whether they extend through the entire plasma membrane or are merely experienced in one leaflet. In the future, such analysis may allow to identify regions of the cellular membrane in which outer leaflet membrane molecules experience a different level of perturbation than transmembrane molecules. These could be, for example, areas where the cytoskeleton is closely adherent to the plasma membrane.

In comparison to sptPALM, which has been performed in dual color as well [27], our approach offers longer average trajectories and a higher localization precision. In addition, our approach does not require simultaneous activation of photoactivatable fluorophores with an additional near UV laser line, which

would add the difficulty of using three different wavelengths in total internal reflection microscopy simultaneously. A disadvantage of our approach is that intracellular proteins cannot be tracked. Since the method described here is based on uPAINT, it achieves similar results, albeit for two membrane probes and using solely the very small, high affinity nanobodies instead of other, larger tags.

Besides SPT, mHoneydew in combination with anti-RFP nanobodies may furthermore be useful as a label for dual color single molecule localization-based superresolution microscopy methods. For example it could reduce undesired background localizations by replacing mCherry which was recently found to blink under buffer-conditions favorable for single molecule superresolution microscopy [38].

Taken together, the presented method is versatile and easy to use as it requires a single cloning step—the exchange of a fluorescent protein variant for mHoneydew on the fusion protein of interest—to study it in conjunction with a second protein of interest, labeled with a GFP variant. At the same time, the small size of the label allows for access to labeling sites even in complex and dense samples where larger labels such as quantum dots may be sterically hindered.

## Acknowledgments

The authors thank all members of the Ewers laboratory for helpful discussions. The authors acknowledge support from the Swiss National Fund, the European Commission Marie Curie Action (FP7-PEOPLE-2013-IEF 630024) (CMW), and the School of Biomedical Sciences of King's College London. The authors declare no competing financial interests.

## References

[1] Kusumi A, Sako Y and Yamamoto M 1993 Confined lateral diffusion of membrane receptors as studied by single particle tracking (nanovid microscopy). Effects of calcium-induced differentiation in cultured epithelial cells *Biophys. J.* **65** 2021–40

[2] Simson R, Sheets E D and Jacobson K 1995 Detection of temporary lateral confinement of membrane proteins using single-particle tracking analysis *Biophys. J.* **69** 989–93

[3] Sako Y and Kusumi A 1994 Compartmentalized structure of the plasma membrane for receptor movements as revealed by a nanometer-level motion analysis *J. Cell Biol.* **125** 1251–64

[4] Borgdorff A J and Choquet D 2002 Regulation of AMPA receptor lateral movements *Nature* **417** 649–53

[5] Nair D, Hosy E, Petersen J D, Constals A, Giannone G, Choquet D and Sibarita J-B 2013 Super-resolution imaging reveals that AMPA receptors inside synapses are dynamically organized in nanodomains regulated by PSD95 *J. Neurosci.* **33** 13204–24

[6] Cognet L, Leduc C and Lounis B 2014 Advances in live-cell single-particle tracking and dynamic super-resolution imaging *Curr. Opin. Chem. Biol.* **20** 78–85

[7] Kusumi A, Fujiwara T K, Chadda R, Xie M, Tsunoyama T A, Kalay Z, Kasai R S and Suzuki K G N 2012 Dynamic organizing principles of the plasma membrane that regulate signal transduction: commemorating the fortieth anniversary of Singer and Nicolson's fluid-mosaic model *Annu. Rev. Cell Dev. Biol.* **28** 215–50

[8] Saxton M J and Jacobson K 1997 Single-particle tracking: applications to membrane dynamics *Annu. Rev. Biophys. Biomol. Struct.* **26** 373–99

[9] Brandenburg B and Zhuang X 2007 Virus trafficking—learning from single-virus tracking *Nat. Rev. Microbiol.* **5** 197–208

[10] Cognet L, Tardin C, Boyer D, Choquet D, Tamarat P and Lounis B 2003 Single metallic nanoparticle imaging for protein detection in cells *Proc. Natl Acad. Sci. USA* **100** 11350–5

[11] Kukura P, Ewers H, Müller C, Renn A, Helenius A and Sandoghdar V 2009 High-speed nanoscopic tracking of the position and orientation of a single virus *Nat. Methods* **6** 923–7

[12] Ortega-Arroyo J and Kukura P 2012 Interferometric scattering microscopy (iSCAT): new frontiers in ultrafast and ultrasensitive optical microscopy *Phys. Chem. Chem. Phys.* **14** 15625–36

[13] Cai E *et al* 2014 Stable small quantum dots for synaptic receptor tracking on live neurons *Angew. Chem. Int. Edn Engl.* **53** 12484–8

[14] Ries J, Kaplan C, Platonova E, Eghlidi H and Ewers H 2012 A simple, versatile method for GFP-based super-resolution microscopy via nanobodies *Nat. Methods* **9** 582–4

[15] Grunwald C, Schulze K, Giannone G, Cognet L, Lounis B, Choquet D and Tampé R 2011 Quantum-yield-optimized fluorophores for site-specific labeling and super-resolution imaging *J. Am. Chem. Soc.* **133** 8090–3

[16] Helmuth J A, Burckhardt C J, Koumoutsakos P, Greber U F and Sbalzarini I F 2007 A novel supervised trajectory segmentation algorithm identifies distinct types of human adenovirus motion in host cells *J. Struct. Biol.* **159** 347–58

[17] Persson F, Lindén M, Unoson C and Elf J 2013 Extracting intracellular diffusive states and transition rates from single-molecule tracking data *Nat. Methods* **10** 265–9

[18] Chenouard N *et al* 2014 Objective comparison of particle tracking methods *Nat. Methods* **11** 281–9

[19] Giannone G *et al* 2010 Dynamic superresolution imaging of endogenous proteins on living cells at ultra-high density *Biophys. J.* **99** 1303–10

[20] Manley S, Gillette J M, Patterson G H, Shroff H, Hess H F, Betzig E and Lippincott-Schwartz J 2008 High-density mapping of single-molecule trajectories with photoactivated localization microscopy *Nat. Methods* **5** 155–7

[21] Douglass A D and Vale R D 2005 Single-molecule microscopy reveals plasma membrane microdomains created by protein–protein networks that exclude or trap signaling molecules in T cells *Cell* **121** 937–50

[22] MacGillavry H D, Song Y, Raghavachari S and Blanpied T A 2013 Nanoscale scaffolding domains within the postsynaptic density concentrate synaptic AMPA receptors *Neuron* **78** 615–22

[23] Rossier O *et al* 2012 Integrins $\beta(1)$ and $\beta(3)$ exhibit distinct dynamic nanoscale organizations inside focal adhesions *Nat. Cell Biol.* **14** 1057–67

[24] Cutler P J, Malik M D, Liu S, Byars J M, Lidke D S and Lidke K A 2013 Multi-color quantum dot tracking using a high-speed hyperspectral line-scanning microscope *PLoS One* **8** e64320

[25] Guzman A, Zelman-Femiak M, Boergermann J H, Paschkowsky S, Kreuzaler P A, Fratzl P, Harms G S and Knaus P 2012 SMAD versus non-SMAD signaling is determined by lateral mobility of bone morphogenetic protein (BMP) receptors *J. Biol. Chem.* **287** 39492–504

[26] Arnspang E C, Brewer J R and Lagerholm B C 2012 Multi-color single particle tracking with quantum dots *PLoS One* **7** e48521

[27] Subach F V, Patterson G H, Renz M, Lippincott-Schwartz J and Verkhusha V V 2010 Bright monomeric photoactivatable red fluorescent protein for two-color super-resolution sptPALM of live cells *J. Am. Chem. Soc.* **132** 6481–91

[28] Shaner N C, Campbell R E, Steinbach P A, Giepmans B N G, Palmer A E and Tsien R Y 2004 Improved monomeric red, orange and yellow fluorescent proteins derived from

Discosoma sp. red fluorescent protein *Nat. Biotechnol.* **22** 1567–72
[29] Keller P, Toomre D, Díaz E, White J and Simons K 2001 Multicolour imaging of post-Golgi sorting and trafficking in live cells *Nat. Cell Biol.* **3** 140–9
[30] Ewers H, Tada T, Petersen J D, Rácz B, Sheng M and Choquet D 2014 A septin-dependent diffusion barrier at dendritic spine necks *PLoS One* **9** e113916
[31] Smith C S, Joseph N, Rieger B and Lidke K A 2010 Fast, single-molecule localization that achieves theoretically minimum uncertainty *Nat. Methods* **7** 373–5
[32] Ormö M, Cubitt A B, Kallio K, Gross L A, Tsien R Y and Remington S J 1996 Crystal structure of the Aequorea victoria green fluorescent protein *Science* **273** 1392–5
[33] Matz M V, Fradkov A F, Labas Y A, Savitsky A P, Zaraisky A G, Markelov M L and Lukyanov S A 1999 Fluorescent proteins from nonbioluminescent Anthozoa species *Nat. Biotechnol.* **17** 969–73
[34] Kenworthy A K, Nichols B J, Remmert C L, Hendrix G M, Kumar M, Zimmerberg J and Lippincott-Schwartz J 2004 Dynamics of putative raft-associated proteins at the cell surface *J. Cell Biol.* **165** 735–46
[35] Pralle A, Keller P, Florin E L, Simons K and Hörber J K 2000 Sphingolipid-cholesterol rafts diffuse as small entities in the plasma membrane of mammalian cells *J. Cell Biol.* **148** 997–1008
[36] Frick M, Schmidt K and Nichols B J 2007 Modulation of lateral diffusion in the plasma membrane by protein density *Curr. Biol.* **17** 462–7
[37] Edidin M, Zúñiga M C and Sheetz M P 1994 Truncation mutants define and locate cytoplasmic barriers to lateral mobility of membrane glycoproteins *Proc. Natl Acad. Sci. USA* **91** 3378–82
[38] Winterflood C M and Ewers H 2014 Single-molecule localization microscopy using mCherry *Chemphyschem* **15** 3447–51